Noname manuscript No.
(will be inserted by the editor)

Masonry elastic characteristics assessment by thermographic images

Federico Cluni · Vittorio Gusella · Gianluca Vinti

Received: date / Accepted: date

Abstract In the present paper, the elastic mechanical characteristics of masonry samples, whose texture is not visible due to plaster, are estimated by means of homogenization technique applied through thermographic images. In particular, three masonry samples with different textures have been purposely built. The textures chosen were periodic, quasi-periodic and random. The images, taken with a thermocamera, have been analyzed in order to identify the texture. An homogenization technique, based on the application of appropriate boundary conditions, has been used. The mechanical characteristics obtained using the textures identified using photographic images and thermographic images have been compared. The influence of some parameters (such as the dimensions of the structural element used in morphological operator) are analysed. The obtained results permits to point out the reliability of the masonry elastic characteristics assessment by the proposed procedure.

F. Cluni
Dept. of Civil and Environmental Engineering, University of Perugia, via G. Duranti 93, 06125 Perugia, Italy
Tel.: +39-075-5853955
E-mail: federico.cluni@unipg.it
*ORCID:*0000-0003-4204-2324

V. Gusella
Dept. of Civil and Environmental Engineering, University of Perugia, via G. Duranti 93, 06125 Perugia, Italy
Tel.: +39-075-5853904
E-mail: vittorio.gusella@unipg.it
*ORCID:*0000-0003-0203-5349

G. Vinti
Dept. of Mathematics and Informatics, University of Perugia, Via Vanvitelli 1, 06123 Perugia, Italy
Tel.: +39-075-5855025
E-mail: gianluca.vinti@unipg.it
*ORCID:*0000-0002-9875-2790

Keywords Homogenization · Masonry Texture · Digital Image Processing · Thermography

1 Introduction

The assessment of the mechanical characteristics of the masonry assumes an important role with particular attention to structural analysis and restoration of historical constructions and cultural heritages.

Considering the masonry as a bi-phase composite, built by mortar and bricks (or stones), the mechanical behaviour is depending on the actual texture, both in elastic field [1,2] and in plastic one [3,4].

An adequate recognition of the texture is necessary to evaluate the Periodic Unit Cell (PUC) in periodic case [5]. This is also true to asses the Representative Volume Element (RVE) for quasi periodic or random arrangements [6,7]. Moreover, the knowledge of the actual texture takes a fundamental role using the approach that involves the periodization of random media by statically equivalent periodic unit cell [8–12]. Eventually the texture knowledge is necessary for the homogenization residuals analysis [13].

Given the previous observations, it is obvious the importance of developing procedures for identifying the texture of the masonry in order to estimate the mechanical characteristics by non destructive testing.

In recent years, the possibility of estimating the masonry texture by means of digital (photographic) images has been explored by several authors [11,14]; moreover digital images can be acquired by laser scanner [15].

These procedures are not applicable when the masonry walls are covered with plaster or, very frequently for historical building, with frescoes.

To overcome these situations, the thermographic tool have recently been proposed in [16,17] where some methods to enhance the images and subsequently to estimate the masonry characteristics are proposed.

Nevertheless a fundamental aspect to be investigated is the reliability assessment of the thermographic procedure for masonry texture recognition. To analysis this topic an ongoing research has been launched with the building of masonry wall samples with different textures and the assessment of mechanical characteristics by homogenization theory based both on photographic and thermographic images.

This paper reports the first obtained results and it is organized in the following sections. After some aspects of the thermographic theory and the peculiarities of the apparatus used in the experimental tests are described in Sec. 2, the characteristics of masonry samples and how they were built are described in Sec. 3 The homogenization approach used to obtain the elastic masonry characteristics is briefly remembered in Sec. 4, and the procedure to identify the texture is recalled in Sec. 5. Finally, the comparison between photographic results and thermographic results is shown in Sec. 6, with comments on the reliability of the proposed procedure.

The influence of some parameters involved in the proposed approach (such as the dimensions of the structural element used in morphological operators) are analyzed.

2 Thermographic images

The principle by which the thermography works is that every body emits electromagnetic radiation, some part of it being in infrared range depending on its temperature. If the sample is not in thermal equilibrium, there is an heat flux which pass trough it: since the thermal conductivity of mortar and bricks are different, the two phases have different temperatures which can be detected by an infrared sensor. Therefore, by means of thermography it is possible to measure the infrared radiation emitted from every body without direct contact, so that it can be considered a non-destructive test technique.

A thermographic camera differs from a photographic camera on the wave lengths of the radiation which it can detect: the wave lengths of the radiation which can be measured by a thermographic camera are in the infrared range, between about 700 nm-1 mm, which correspond to 430 THz-300 GHz in frequency, while the wave lengths of the radiation which can be measured by a photographic camera are in the visible range, between about 400 nm-700 nm, which correspond to 190 GHz-430 GHz, see Fig. 1

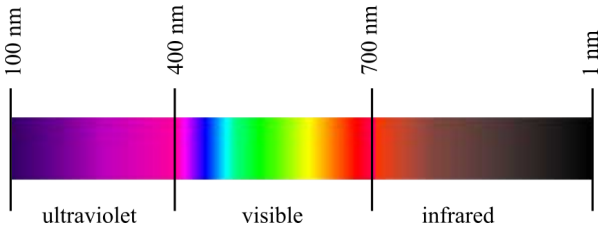

Fig. 1 Radiation wave length range.

The image resolution is typically much smaller than that allowed by a photographic camera, and therefore reconstruction technique could be used to enhance the quality of the image [16,17]. In the present paper, two thermocamera models have been used: the thermocamera model B360 from FLIR has been used for the quasi-periodic masonry sample and model 885-2 from Testo has been used for periodic and random masonry samples. Each of the model have a sensor of dimension 320×240 pixels. All the samples have been exposed to direct sunlight in order to improve the heat flux trough the body.

3 Building of samples

Three samples of masonry walls have been built; for all the samples, UNI bricks of dimensions 250×120×55 mm have been employed, either used as a whole or split in two or in four, as shown in Fig. 2. Mortar joint were made 1 mm in thickness.

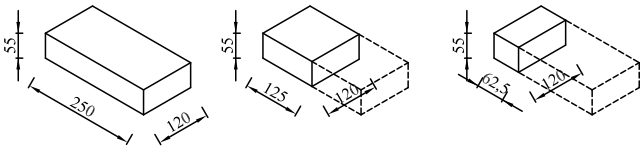

Fig. 2 Bricks used to build the samples.

In what follows, we denote width of the brick its horizontal length, height of the brick its vertical length. The bricks were assembled using three different textures:

(i) a periodic texture, made with brick having the same widths and heights. In particular, a running bond texture has been used, where head joints of adjacent rows are half brick width apart;
(ii) a quasi-periodic texture, made with bricks having different widths but equal heights, arranged in horizontal rows in such a way to avoid the correspondence between vertical joints ;

(iii) a random texture, made using bricks having different widths and heights (achieved by rotating some bricks).

The texture's typologies of the masonry wall are shown in Fig. 3. For periodic and random textures, samples whit 780 x 780 mm dimensions were built. The sample of quasi-periodic masonry has been built larger than the others, with 835 x 780 mm dimensions. In Fig. 3 the actual portion of samples is shown inside the dashed line.

The masonry samples, as built before the application of the plaster, are shown in Fig. 4. As a final step, the samples have been covered with plaster, as can be seen in Fig. 5(a) for the quasi-periodic texture sample. An example of the image of the sample with quasi-periodic masonry obtained bt the thermocamera is shown in Fig. 5(b).

4 Homogenization of masonry

The mechanical characteristics of the masonry have been estimated as in [6]. The procedure is here recalled briefly. We recall that we are in a case of plain stress, and therefore

$$\sigma_{zz} = \sigma_{xy} = \sigma_{yz} = 0 \tag{1}$$

With the preceding, the relation between stress and strain can be expressed, using Voigt notation, with the following

$$\sigma = C\epsilon \tag{2}$$

where C is a symmetric square matrix denoted *stiffness matrix*

$$C = \begin{bmatrix} C_{11}\ C_{12}\ C_{13} \\ C_{12}\ C_{22}\ C_{23} \\ C_{13}\ C_{23}\ C_{33} \end{bmatrix} \tag{3}$$

and

$$\sigma = \{\sigma_{xx}, \sigma_{yy}, \sigma_{xy}\}^T, \quad \epsilon = \{\epsilon_{xx}, \epsilon_{yy}, 2\epsilon_{xy}\}^T \tag{4}$$

Instead of stiffness matrix, the *flexibility matrix* S can be used

$$\epsilon = S\sigma \tag{5}$$

with

$$S = \begin{bmatrix} S_{11}\ S_{12}\ S_{13} \\ S_{12}\ S_{22}\ S_{23} \\ S_{13}\ S_{23}\ S_{33} \end{bmatrix} \tag{6}$$

Obviously, $S = C^{-1}$. In the case of orthotropic material, $C_{13} = C_{23} = S_{13} = S_{23} = 0$.

Since the material is heterogeneous, the relations (2 and (5) are in terms of mean values averaged over the volume Ω as follows

$$\langle\sigma\rangle = C^H\langle\epsilon\rangle, \quad \langle\epsilon\rangle = S^H\langle\sigma\rangle \tag{7}$$

where

$$\langle\sigma\rangle = \frac{1}{|\Omega|}\int_\Omega \sigma d\Omega, \quad \langle\epsilon\rangle = \frac{1}{|\Omega|}\int_\Omega \epsilon d\Omega \tag{8}$$

In (7), C^H is the effective stiffness matrix and S^H is the effective flexibility matrix. In general, if the domain is not the size of a representative volume element, the estimates of C^H and S^H depends on the boundary conditions applied [18]. Two type of boundary conditions are mainly used:

(i) essential boundary conditions, expressed in terms of displacements as

$$\begin{cases} u_x = \epsilon^0_{xx}\, x + \epsilon^0_{xy}\, y \\ u_y = \epsilon^0_{xy}\, x + \epsilon^0_{yy}\, y \end{cases} \tag{9}$$

where (x, y) are the coordinates of the point on the boundary. By imposing $\left\{\epsilon^0_{xx}, \epsilon^0_{yy}, 2\epsilon^0_{xy}\right\}^T = \{1, 0, 0\}^T$ we have $\langle\epsilon\rangle = \{1, 0, 0\}^T$ [19] and therefore the first column of the estimate of C^H is given by $\langle\sigma\rangle$. Proceeding in analogous way the other column of the estimate of C^H can be found. This estimate of C^H is denoted by C^E.

(ii) natural boundary conditions, expressed in terms of forces as

$$\begin{cases} t_x = \sigma^0_{xx}\, n_x + \sigma^0_{xy}\, n_y \\ t_y = \sigma^0_{xy}\, n_x + \sigma^0_{yy}\, n_y \end{cases} \tag{10}$$

where (n_x, n_y) denotes the outward normal vector at the point on the boundary. By imposing $\left\{\sigma^0_{xx}, \sigma^0_{yy}, \sigma^0_{xy}\right\}^T = \{1, 0, 0\}^T$ we have $\langle\sigma\rangle = \{1, 0, 0\}^T$ [19] and therefore the first column of the estimate of S^H is given by $\langle\epsilon\rangle$. Proceeding in analogous way the other column of the estimate of S^H, and therefore the estimate of C^H as $C^H = \left(S^H\right)^{-1}$ can be found. This estimate of C^H is denoted by C^N

It is possible to prove that [20]

$$C^N \leq C^H \leq C^N \tag{11}$$

In case that C^E and C^N are sufficiently close, C^H can be estimated through the following arithmetic mean:

$$C^H = \frac{1}{2}\left(C^E + C^N\right) \tag{12}$$

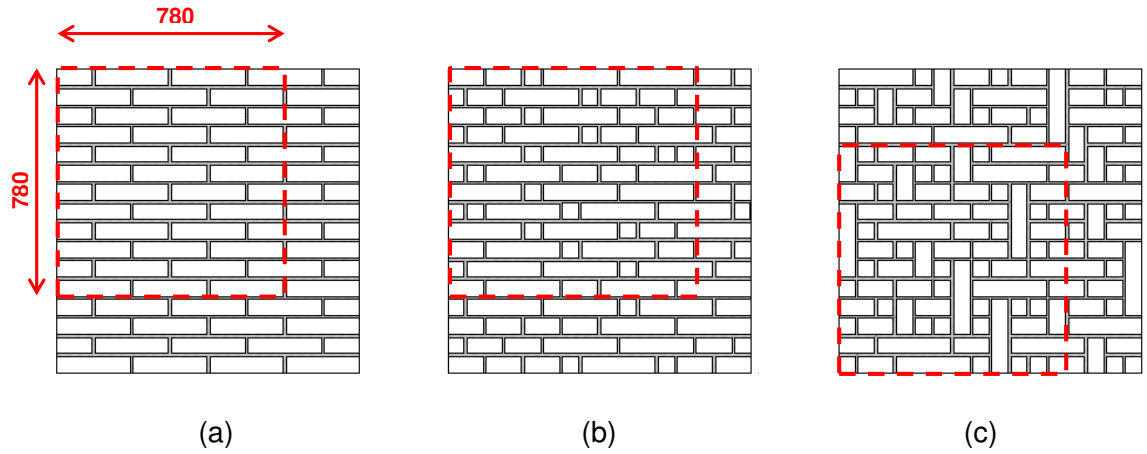

Fig. 3 Textures of masonry wall samples: periodic (a), quasi-periodic (b) and random (c).

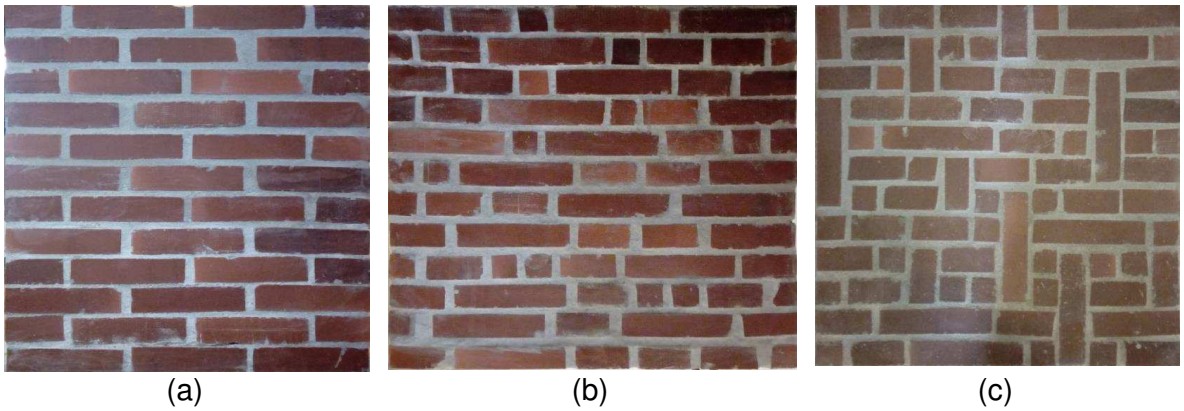

Fig. 4 Masonry wall samples: periodic (a), quasi-periodic (b) and random (c).

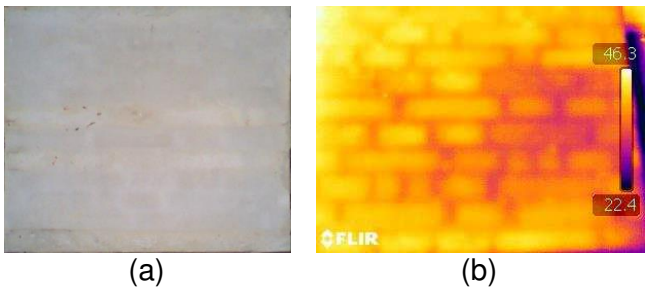

Fig. 5 Quasi-periodic masonry wall sample covered with plaster (a) and its thermographic image (b).

5 Identification of texture

The estimation of the texture from the photographic and the thermographic images follows the same steps. In particular, the images are converted from color images to black and white images [17], in which black pixels identify mortar elements and white pixels identify brick elements. It is worth noting that, if necessary, the image was corrected in order to compensate the perspective.

An image can be seen as one or more discrete functions, $f_i(x, y)$, with $x = 1, 2, \ldots, N$ and $y = 1, 2, \ldots, N$, where N is the image width in pixels (it is assumed that the image has equal width and height). In case of color image, there are three functions f_i, one for each channel (red, green and blue). In case of gray-scale image, there is only one function, corresponding to the gray level (usually expressed in the range 0-1).

At first the image is converted from color to gray-scale by eliminating hue and saturation information while retaining the luminance [21]. In particular the following function is used

$$g(x, y) = 0.299\, f_R(x, y) + 0.587\, f_G(x, y) + \\ + 0.114\, f_B(x, y) \quad (13)$$

where $g(x, y)$ is the gray level of the pixel at position (x, y) and $\{f_R, f_G, f_B\}$ are the red, green and blue levels of the same pixel in the color image.

Thereafter a median filter to enhance the quality of image is applied. The median filter is defined by the

following

$$\bar{g}(x,y) = \text{median}\left\{ g(s,t) \text{ for } (s,t) \text{ in } N^l_{(x,y)} \right\} \tag{14}$$

where $N^l_{(x,y)}$ is a structural element, a square of side l pixels center in pixel at (x,y). In the present case, l =3.

The gray-scale image is converted to a black and white image by the following

$$b(x,y) = \begin{cases} 0 \text{ if } \bar{g}(x,y) \leq k \\ 1 \text{ if } \bar{g}(x,y) > k \end{cases} \tag{15}$$

where k is the gray level used as a threshold. In the current application, the value of k is chosen using an adaptive approach [22] in order to compensate the effect of gradient of illumination present in the images. The value 1 (black) is associated with mortar pixels, the value 0 (white) with brick pixels.

As final steps, morphological operators are used. At first, mortar (black) region of pixels which are surrounded by brick (white) pixels are removed. Finally erosion and dilation operators are applied (in this succession) in order to smooth the contours of the inclusions.

In particular, erosion is defined by

$$b_e(x,y) = \text{maximum}\left\{ b(s,t) \text{ for } (s,t) \text{in} N^l_{(x,y)} \right\} \tag{16}$$

and dilation by

$$b_d(x,y) = \text{minimum}\left\{ b_e(s,t) \text{ for } (s,t) \text{in} N^l_{(x,y)} \right\} \tag{17}$$

The resulting black and white image has a consistent separation of phases, i.e. each stone is surrounded by mortar joints and unrealistic conjunction of inclusions is reduce as much as possible.

A portion with eight rows of stones and with a width equivalent to two entire bricks has been chosen, together with the corresponding head and bed joints, therefore the dimensions of the portion are 520 mm in width and 520 mm in height. The corresponding image size in pixel is 200×200.

In Figs. 6-8, the obtained results for both the thermographic image and the photographic image of the same portion of sample is shown. In particular, in the case of thermographic images two different black and white images image have been obtained, differing in the value of l used for dilation operator: $l = 3$ is the same used for erosion, $l = 5$ is slightly larger and used in order to obtain a concentration ratio, defined as the percentage of brick phase, closer to the one of photographic image.

Phase	Young's modulus [MPa]	Poisson ratio
Brick	20000	0.2
Mortar	5000	0.2

Table 1 mechanical characteristics of constituent phases

	c_1	C_{11}	C_{12}	C_{22}	C_{33}
Natural b.c.					
Photographic	0.684	13708	2225	11333	4417
Therm. $l = 3$	0.482	10482	1770	8651	3433
Therm. $l = 5$	0.592	12071	2022	9989	3948
Essential b.c.					
Photographic	0.684	14024	2243	11496	4539
Therm. $l = 3$	0.482	10831	1794	8848	3533
Therm. $l = 5$	0.592	12490	2051	10234	4080
Effective					
Photographic	0.684	13866	2234	11415	4478
Therm. $l = 3$	0.482	10657	1782	8749	3483
Therm. $l = 5$	0.592	12280	2036	10111	4014

Table 2 Concentration ratio (non-dimensional) and components of estimated stiffness matrix for periodic texture (in MPa).

	c_1	C_{11}	C_{12}	C_{22}	C_{33}
Natural b.c.					
Photographic	0.620	12285	2050	10425	4044
Therm. $l = 3$	0.538	10803	1928	9446	3709
Therm. $l = 5$	0.646	12468	2209	11053	4304
Essential b.c.					
Photographic	0.620	12606	2064	10597	4163
Therm. $l = 3$	0.538	11173	1944	9692	3846
Therm. $l = 5$	0.646	12837	2231	11308	4455
Effective					
Photographic	0.620	12446	2057	10511	4103
Therm. $l = 3$	0.538	10988	1936	9569	3778
Therm. $l = 5$	0.646	12653	2220	11181	4379

Table 3 Concentration ratio (non-dimensional) and components of estimated stiffness matrix for quasi-periodic texture (in MPa).

6 Numerical results

In order to obtain the estimates of C^E and C^N, the boundary value problems are solved through finite element method using 4-node elements with plane stress formulation, assuming that each pixel of the binary image is a finite element.

The mechanical characteristics used for the constituent phases are reported in Tab. 1.

The results in terms on components of stiffness matrix are shown in Tab. 2-4.

In all of the cases the difference between the estimates in natural and essential boundary conditions are

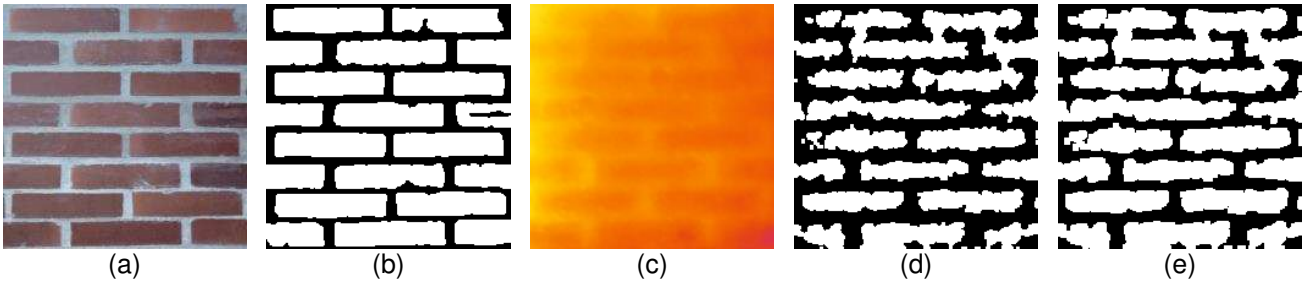

Fig. 6 Identified texture of periodic masonry sample: photographic image image (a) and its identified texture, thermographic image (c) and its identified texture with $l = 3$ (d) and $l = 5$ (e).

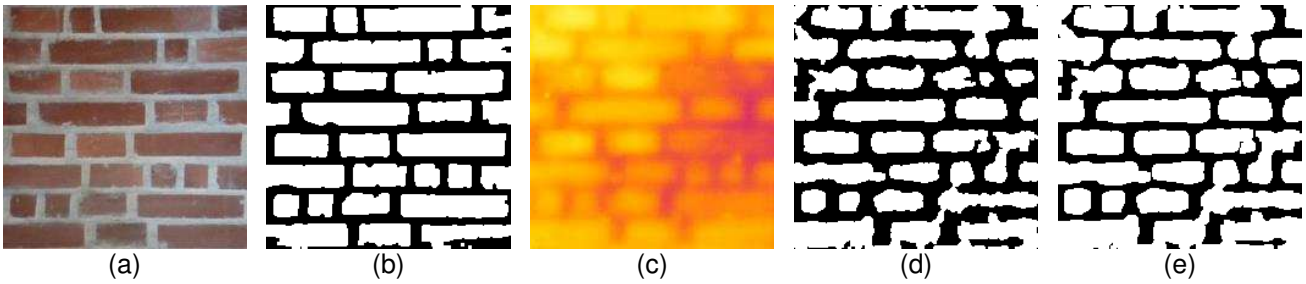

Fig. 7 Identified texture of quasi-periodic masonry sample: photographic image image (a) and its identified texture, thermographic image (c) and its identified texture with $l = 3$ (d) and $l = 5$ (e).

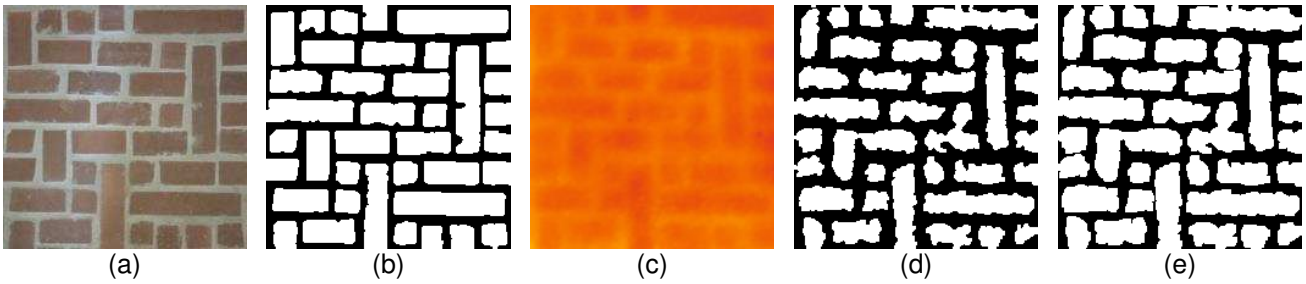

Fig. 8 Identified texture of random masonry sample: photographic image image (a) and its identified texture, thermographic image (c) and its identified texture with $l = 3$ (d) and $l = 5$ (e).

below the 3%, and therefore the portion of the sample is close to the representative volume element. As expected, the results show a dependency not only on the texture but also on the concentration ratio, c_1. The difference is about 25% for $l = 3$ and 12% for $l = 5$ in the case of periodic texture, 11% for $l = 3$ and 5% for $l = 5$ in the case of quasi-periodic texture, while is about 17% for $l = 3$ and 4% for $l = 5$ in the case of random texture.

The information contained in the stiffness matrix, and in its inverse the flexibility matrix, can be used to estimate the value of the engineering constants involved in orthotropic materials, E_x, E_y, ν_{xy} and G_{xy} and their mutual relation. In particular, in plane stress the flexibility matrix can be written as

$$S = \begin{bmatrix} \frac{1}{E_x} & -\frac{\nu_{xy}}{E_x} & 0 \\ -\frac{\nu_{xy}}{E_x} & \frac{1}{E_y} & 0 \\ 0 & 0 & \frac{1}{Gxy} \end{bmatrix} \tag{18}$$

and the stiffness matrix can be written as

$$C = \begin{bmatrix} \frac{E_x^2}{E_x - E_y\,\nu_{xy}^2} & \frac{E_x\,E_y\,\nu_{xy}}{E_x - E_y\,\nu_{xy}^2} & 0 \\ \frac{E_x\,E_y\,\nu_{xy}}{E_x - E_y\,\nu_{xy}^2} & \frac{E_x\,E_y}{E_x - E_y\,\nu_{xy}^2} & 0 \\ 0 & 0 & Gxy \end{bmatrix} \tag{19}$$

The values of the engineering constants E_x, E_y and ν_{xy} can be found by the following

$$E_x = \frac{1}{S_{11}}, \quad E_y = \frac{1}{S_{22}}, \quad \nu_{xy} = -\frac{S_{12}}{S_{11}} \tag{20}$$

	c_1	C_{11}	C_{12}	C_{22}	C_{33}
Natural b.c.					
Photographic	0.642	12128	2076	11215	4154
Therm. $l = 3$	0.496	9878	1788	9289	3485
Therm. $l = 5$	0.610	11481	2042	10831	4037
Essential b.c.					
Photographic	0.642	12355	2085	11404	4262
Therm. $l = 3$	0.496	10137	1796	9503	3575
Therm. $l = 5$	0.610	11778	2057	11085	4151
Effective					
Photographic	0.642	12241	2080	11310	4208
Therm. $l = 3$	0.496	10008	1792	9396	3530
Therm. $l = 5$	0.610	11629	2049	10958	4094

Table 4 Concentration ratio (non-dimensional) and components of estimated stiffness matrix for random texture (in MPa).

	c_1	E_x	E_y	ν_{xy}	G_{xy}
Periodic					
Photographic	0.684	13428	11055	0.196	4478
Therm. $l = 3$	0.482	10293	8452	0.204	3483
Therm. $l = 5$	0.592	11869	9774	0.201	4014
Quasi-periodic					
Photographic	0.620	12043	10171	0.196	4103
Therm. $l = 3$	0.538	10596	9228	0.202	3778
Therm. $l = 5$	0.646	12212	10791	0.199	4379
Random					
Photographic	0.642	11859	10956	0.184	4208
Therm. $l = 3$	0.496	9666	9075	0.191	3530
Therm. $l = 5$	0.610	11246	10597	0.187	4094

Table 5 Concentration ratio (non-dimensional) and estimated value of engineering constants (E_x, E_y and G_{xy} in MPa).

The results are show in Tab. 5

Moreover, the following relation between the engineering constants can be established

$$\frac{E_x}{E_y} = \frac{C_{11}}{C_{22}}, \quad \nu_{xy} = \frac{C_{12}}{C_{22}}, \quad \frac{G_{xy}}{E_x} = \frac{C_{33}}{C_{11}} \tag{21}$$

and the results are show in Tab. 6.

As can be seen, the results in terms of ratio of engineering constants are in good agreement, since the effect of phase concentration is greatly reduced. Therefore, in terms of characterization of the orthotropic behavior the estimates that can be made using thermographic images can be considered quite reliable.

	c_1	E_x/E_y	ν_{xy}	G_{xy}/E_x
Periodic				
Photographic	0.684	1.215	0.196	0.323
Therm. $l = 3$	0.482	1.218	0.204	0.327
Therm. $l = 5$	0.592	1.214	0.201	0.327
Quasi-periodic				
Photographic	0.620	1.184	0.196	0.330
Therm. $l = 3$	0.538	1.148	0.202	0.344
Therm. $l = 5$	0.646	1.132	0.199	0.346
Random				
Photographic	0.642	1.082	0.184	0.344
Therm. $l = 3$	0.496	1.065	0.191	0.353
Therm. $l = 5$	0.610	1.061	0.187	0.352

Table 6 Relation between engineering constants.

7 Conclusions

In the present paper we present the first results of an ongoing research relative to estimation of the mechanical characteristics of masonry walls covered with plaster using nondestructive techniques. The method is based on a thermographic image of the masonry, to which digital image techniques are applied in order to obtain a black and white image with a consistent separation of the phases (brick and mortar in the present case study). Then, the mechanical characteristics are estimated by means of an homogenization procedure based on natural and essential boundary conditions. These mechanical characteristics have been compared with those obtained using a photographic image of the same sample with a good agreement; then the obtained results highlight the reliability of thermographic procedure. As a further development, it is planned that the research will continue with laboratory tests on the masonry walls samples described in the present paper to experimentally estimate their elastic characteristics, in order to provide a validation of the proposed procedures.

Acknowledgments

Authors gratefully acknowledge the support received from the Italian Ministry of University and Research, through the PRIN 2015 funding scheme (project 2015 JW9NJT - Advanced mechanical modelling of new materials and structures for the solution of 2020 Horizon challenges).

References

1. Anthoine A (1995) Derivation of the in-plane elastic characteristics of masonry through homogenization theory. Int J Solids Struct 32:137–163
2. Lombardo M, Zeman J, Šejnoha M, Falsone G. (2015) Stochastic modeling of chaotic masonry via mesostructural characterization. International Journal for Multiscale Computational Engineering 7(2):171–185
3. Cavalagli N, Cluni F, Gusella V (2011) Strength domain of non-periodic masonry by homogenization in generalized plane state. Eur J Mech A-Solid 30:113–126

4. Casolo S, Milani G (2013) Simplified out-of-plane modelling of three-leaf masonry walls accounting for the material texture. Constr Build Mater 40:330–351
5. Cecchi A, Sab K (2002) A multi-parameter homogenization study for modeling elastic masonry, Eur J Mech A-Solid 21:249–268
6. Cluni F, Gusella V (2004) Homogenization of non-periodic masonry structures. Int J Solids Struct 41:1911–1923
7. Gusella V, Cluni F (2006) Random field and homogenization for masonry with nonperiodic microstructure. J Mech Mat Struct 1:357–386
8. Sab K, Nedjar B (2005) Periodization of random media and representative volume element size for linear composites, CR Mecanique 333:187–195
9. Šejnoha J, Šejnoha M, Zeman J, Sykora J, Vorel J (2008) Mesoscopic study on historic masonry. Struct Eng Mech 30:99–117
10. Zeman J, Šejnoha M. (2007) From random microstructures to representative volume elements. Modelling and Simulation in Materials Science and Engineering 15 (4):325–35.
11. Cavalagli N, Cluni F, Gusella V (2013) Evaluation of a Statistically Equivalent Periodic Unit Cell for a quasi-periodic masonry. Int J Solids Struct 50:4226-4240
12. Cavalagli N, Cluni F, Gusella V (2018) Failure surface of quasi-periodic masonry by means of Statistically Equivalent Periodic Unit Cell approach. Meccanica 53:1719–1736
13. Cluni F, Gusella V (2018) Estimation of residuals for the homogenized solution of quasi-periodic media. Probab Eng Mech 54:110–117
14. Falsone G, Lombardo M (2009) Stochastic representation of the mechanical properties of irregular masonry structures. Int J Solids Struct 44:8600–8612
15. Milani G, Esquivel YW, Loureno PB, Riveiro B, Oliveira DV (2013) Characterization of the response of quasi-periodic masonry: Geometrical investigation, homogenization and application to the Guimarães castle, Portugal. Eng Struct 56:621–641
16. Cluni F, Costarelli D, Minotti AM, Vinti G (2015) Enhancement of thermographic images as tool for structural analysis in earthquake engineering, NDT&E Int 70:60–72
17. Cluni F, Costarelli D, Minotti AM, Vinti G (2015) Applications of sampling Kantorovich operators to thermographic images for seismic engineering. J Comput Anal Appl 19:1–16
18. Hill R (1963) Elastic properties of reinforced solids: Some theoretical principles. J Mech Phys Solids 11:357–372
19. Aboudi, J (1991) Mechanics of Composite Materials: A Unified Micromechanical Approach. Elsevier, Amsterdam.
20. Huet C (1990) Application of variational concepts to size effects in elastic heterogeneous bodies. J Mech Phys Solids 38:813–841.
21. MATLAB and Digital Image Processing Toolbox (2008), The MathWorks, Inc., Natick MA, United States.
22. Gonzales R, Woods R (2002) Digital Image Processing, Prentice-Hall Upper Saddle River NJ, United States.